Scanning Tunneling Microscopy Imaging and Selective Modification of Purple Membranes

R. García,[1] J. Tamayo,[1] C. Bustamante[2]

[1]Instituto de Microelectrónica de Madrid, CSIC, Parque Tecnológico de Madrid, c/Isaac Newton 8, 28760 Tres Cantos, Madrid, Spain

[2]Institute of Molecular Biology, University of Oregon, Eugene, OR 97403, USA

Received 1 July 1996; revised 9 September 1996

ABSTRACT: The invention and development of the scanning tunneling microscope (STM) have opened new and original approaches for atomic- and nanometer-scale studies of surfaces. However, its application for imaging biomolecules has to overcome the poor electrical conductivity of biological samples. This article describes an operation mode of the STM that allows high-resolution imaging of hydrated purple membranes and their selective modification. The imaging requires very low currents (below 1 pA) and applied voltages above 5 V. This mode also allows performance of nanometer-scale modifications of the membranes. These modifications are generated by removing the proteins and lipids from a selected region of the membrane. The removal takes place by establishing tip–membrane mechanical contact. This happens when the operating current is above 2 pA. These experiments pose the problem of electron transport through 5–10-nm-thick insulating materials. We propose a model in which the contrast mechanism is controlled by two factors: the electric field at the interface and the transmission through empty states in the membrane. We also compare these results with STM experiments imaging DNA molecules deposited on insulating substrates. There, the contrast is based on the lateral conductivity of water films. © 1997 John Wiley & Sons, Inc. Int J Imaging Syst Technol, **8,** 168–174, 1997

Key words: STM; field emission; purple membrane; nanotechnology

I. INTRODUCTION

In scanning tunneling microscopy (STM), a sharp, conductive tip follows, from a few angstroms away, the topography of a sample surface while keeping a constant current [Fig. 1(a)]. The scanning tunneling microscope is a powerful tool for imaging [1] and modification [2] of metallic, semimetallic, and semiconductor surfaces at atomic and nanometer scales. Atomic resolution images can be obtained in air, in ultrahigh vacuum, and under liquid environments.

Three-dimensional imaging, atomic resolution, and operations underwater have prompted the application of STM for imaging biomolecules. A variety of organic and biological molecules have been examined by STM [3]. DNA bases [4], DNA [5], DNA–protein complexes [6], globular and elongated proteins [7–9], several protein membranes [10–12], and microtubules [13] are some examples of biomolecules studied by STM. However, those experiments have to deal with the poor electrical conductivity of biomolecules that makes it difficult to establish a constant current. They also pose the problem of the contrast mechanism that allows their imaging by STM.

Several models and calculations based on the coupling between substrate and molecule orbitals [14], resonant tunneling [15], or the modulation of the effective barrier by polarizable molecular adsorbates [16] give some reasonable explanations of the observed contrast for very thin organic films (below 1 nm). The situation is more complicated when biomolecules are involved, and direct tunneling through them gives a negligible contribution to the total current. The experiments themselves are somehow controversial. In some cases, experimental results have been difficult to reproduce, and the factors that contribute to image formation were not properly isolated [17]. On the other hand, the electrical conductivities of some organic films implied by STM observations ($\sim 10^{-2}\ \Omega^{-1}\ \mathrm{cm}^{-1}$) are several orders of magnitude higher than previous macroscopic measurements [18,19]. In general, the mechanisms of electron transport operating in STM experiments involving several-nanometer-thick macromolecules are not known.

In this article, we have chosen purple membranes (PM) as a model system to examine the conditions for reproducible STM imaging of biological specimens. PM are imaged with vertical and lateral resolution of 0.3 and 15 nm, respectively. Successful imaging of PM deposited on conductive supports requires currents below 1 pA and applied voltages above 5.5 V [20]. Based on the experimental results, we propose a model in which the imaging is controlled by the electrical field at the interface and the existence of empty electronic states in the membrane. The tip–sample distance is controlled by the applied voltage and cur-

Correspondence to: R. García

Contract grant sponsor: Dirección General de Investigación Científica y Técnica of Spain; *Contract grant number:* PB94-0016

CCC 0899–9457/97/020168-07

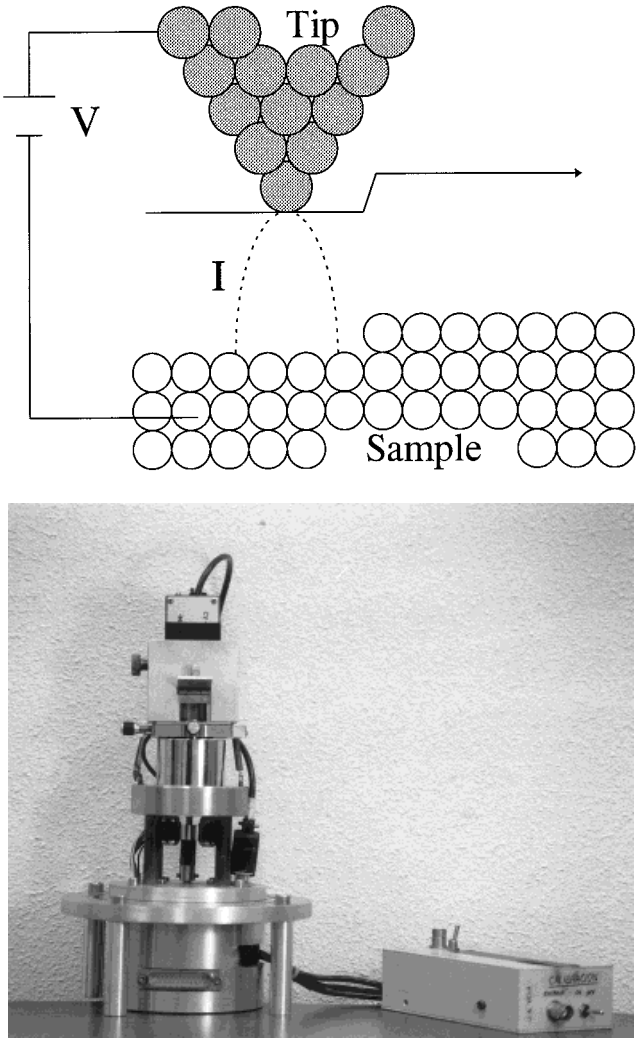

Figure 1. (a) Schematic cross-section of an STM interface. The upper component represents the probe (tip) and the bottom is the sample under examination. *V* and *I* are the applied voltage and the electronic current, respectively. The line with an arrow indicates the scanning direction. (b) Custom-built low-current STM. The patch clamp amplifier is attached to the top of the tip-holder housing. At its bottom there is an *X*–*Y* table for fine positioning of the tip on the sample surface. The tip-holder housing rests on the piezoelectric scanner cradled in the microscope base. The small window allows optical tip–sample coarse approach.

rent. By monitoring those parameters, a method to generate nanometer-scale patterns on the membranes is also presented.

The STM offers a variety of mechanisms to study biomolecules. As an example, we will briefly discuss recent experiments imaging DNA molecules deposited onto insulating substrates [21]. In this case, the lateral conductivity of water films adsorbed onto the biomolecules and on the substrate has a dominant role in the imaging contrast.

II. MATERIALS AND METHODS

Purple membrane is a natural membrane crystal present in the cell membrane wall of halobium bacteria. The membranes used in this study have been obtained following the procedure described in Ref. 22. Its structure has been characterized by electron microscopy and diffraction [23] and recently by atomic force microscopy [24]. The purified membranes appear as oval sheets of about 1 μm diameter and about 5 nm thickness.

Purple membrane is made of a single protein species, *Bacteriorhodopsin.* The proteins are packed in hexagonal symmetry, space group p3, with lattice parameter 6.3 nm. Biologically, the protein acts as a light-driven proton pump. Owing to its structural stability in a wide range of environmental conditions, and to its remarkable optical properties, PM is drawing interest for its potential applications as a high-performance component of optical computers [25].

Highly oriented pyrolitic graphite (HOPG) is used as a solid, conductive support (substrate) for the membranes. HOPG has been extensively studied by STM. It is easily cleaved and inert, offering large, atomically flat regions for deposition. In addition to the above properties, graphite has no structural defects that could resemble the membranes' shape.

Approximately 10 μl of an aqueous suspension of PM (0.1 mg/ml) are sprayed onto the substrate. The graphite is placed perpendicular to the stream and about 10 cm away from the atomizer. The spreading produces small droplets on the graphite that rapidly evaporate, leaving the PM on the surface. The process is repeated several times to guarantee uniform coverage of the surface.

Without any further preparation, the sample is loaded into a special STM chamber that allows control of the relative humidity from 5 to 100%.

A relevant factor for imaging PM is the geometry of the tip. Platinum-iridium electrochemically etched tips were used (Materials Analytical Services, Raleigh, NC). These tips have a high aspect ratio. For some of them, curvature radii as small as 10 nm were measured.

For the DNA, a drop of 10 μl of a solution of 2 μg/ml of double-stranded circular DNA was deposited over 30 s on a freshly cleaved piece of mica, then rinsed in pure water. DNA molecules were imaged with electrochemically etched tungsten tips.

The experiments were performed with a custom-built low-current STM which has two main components: a probe housing that contains the tip holder and carries the low-current amplifier electronics, and the scanner support base which houses electrical connections and the stepper motor for automated approach of the tip to the sample surface [26] [Fig. 1(b)]. This STM can be operated at currents as low as 0.06 pA. The images are taken in the constant current mode. They are raw data with no filtering other than the substration of the background plane.

III. RESULTS AND DISCUSSION

A. Purple Membrane on Graphite. Figure 2 is a topographic image of an uncoated PM sheet on HOPG. The STM current *I* and applied voltage *V* are 0.2 pA and −8 V (sample negative), respectively. The membranes are fixed to the substrate by structural defects such as steps. This is illustrated in the image, where a monoatomic step can be seen running transversely underneath a membrane. Under the present imaging conditions the estimated lateral resolution is about 15 nm. This value is deduced by measuring the width of the cracks and holes of the membranes. The membrane height can be determined from cross-sectional measurements [Fig. 2(b)]: in this image, 5.2 ± 0.4 nm, i.e., in close agreement with previous measurements by other techniques [23].

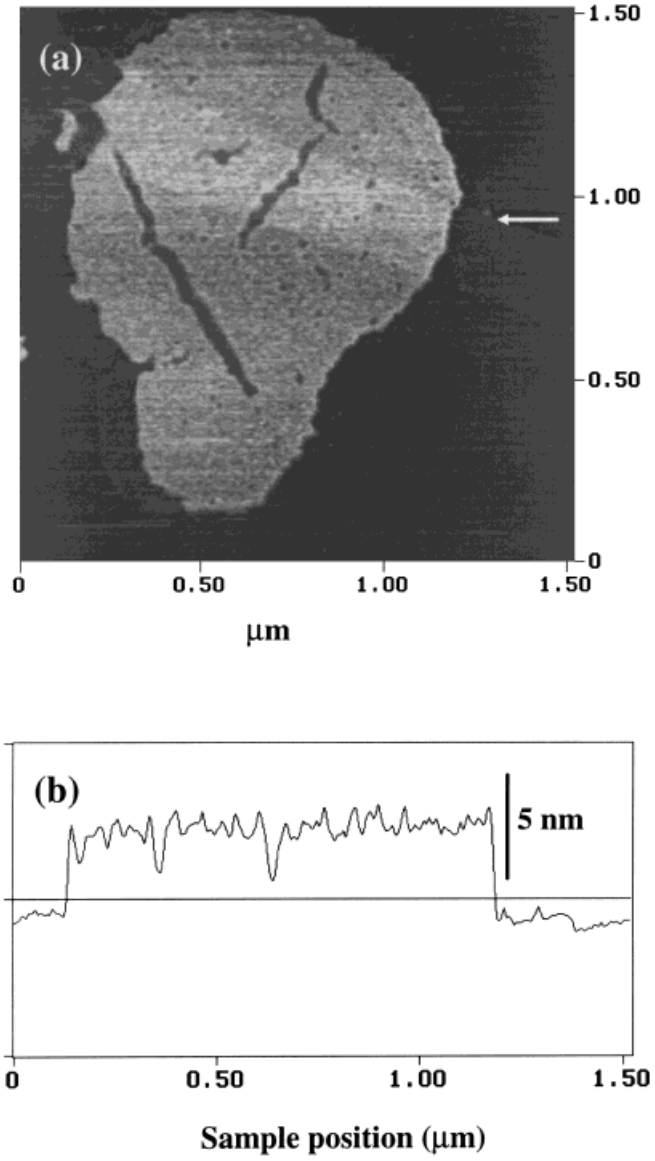

Figure 2. (a) Topographic STM image of a hydrated purple membrane deposited on graphite. Several cracks occurring during air-drying are visible. Scan size: 1.52 × 1.52 μm. Sample voltage: −8 V; tunneling current: 0.2 pA; relative humidity: 42%. (b) Cross-section along the line marked by an arrow in (a).

However, in general, the apparent height of the membrane will depend on the initial tip–substrate separation. This aspect will be discussed in the next section.

Purple membranes have been imaged at both voltage polarities; however, negative polarities are preferred. The lateral resolution is better for that polarity, because tip–substrate distances are smaller. Furthermore, occasional fragmentation of PM has been observed when electrons are emitted from the tip.

We studied the imaging as a function of the set current and applied voltage. First, PM were imaged at different currents while the applied voltage remained constant. The PM shown in Figure 3(a) was imaged at $I = 0.2$ pA and $V = -8$ V. The pattern in Figure 3(b) was generated by scanning that region at 20 pA while keeping the voltage at −8 V. Operation of the STM at 20 pA produces the total removal of the proteins in the scanned region. Further experiments determined that no more than 2 ± 1 pA can be carried through the membrane before tip–sample contact takes place. This current is distributed over an area πr^2, where r is defined by the effective lateral resolution ($r = L_{\text{eff}}/2$). This amounts to a current density of 0.64 A/cm^2, i.e., five orders of magnitude smaller than the current densities measured in STM experiments on metals.

The explanation of the above behavior is straightforward. At operating currents above 2 pA, the electrical impedance of the interface is larger than the ratio between applied voltage and current. To keep the current constant, the feedback approaches the tip toward the sample. This decreases the electrical impedance of the interface, but in many cases it also implies tip–sample mechanical contact. A similar behavior has been observed with cadmium stearate bilayers [27].

In the second type of experiments, PM are imaged at different voltages while the current is kept constant. The results show that partial removal of the proteins starts when the applied voltage is −5 V. At −4 V all proteins of the scanned region are removed from it. They are seen to be piled up to the sides of the stripped region [20]. In short, PM can be successfully imaged for currents below 2 pA and applied voltages above 5.5 V.

Figure 3(b) also illustrates a practical method for performing nanometer-scale modification of biomolecules [28,29]. The average width of the letter written on the membrane is 15 nm. The lateral dimensions of the mark are determined by the tip's aspect ratio and the size of the region where tip and sample are in mechanical contact. The cohesive properties of the lipids within the membrane could define a minimum size, though. The attempt to write 10-nm marks did not produce permanent modifications.

In Figure 4 the PM appears as a depression instead of a protrusion from the substrate surface. This is called negative contrast. It implies that for a given tip–substrate separation (always higher than the thickness of the membrane), the effective electrical impedance when the tip is over the PM is higher than when the tip is over the substrate. In the constant current mode, this is compensated by a reduction of the tip–sample distance when the tip moves from bare graphite to the membrane (between 1 and 4 nm).

Negative contrast implies extremely large tip–substrate separations (above 10 nm), so there is no mechanical contact. It also implies blunt tips. Tips that produce negative contrast have consistently larger radii than their counterparts. This is in agreement with field emission calculations that for negative polarities show an increase of the tip–substrate distance with the curvature radius of the tip [28,29]. A theoretical interpretation of negative/positive contrast images and its dependence on tip–substrate separation will be provided in the next section.

Purple membranes are better observed for relative humidities between 15 and 60%. At low relative humidities (RH) there is partial fading of the membranes in the image. The origin of this effect is not yet clear. We speculate that it could be related to changes in the dielectric response of the membrane with water absorption. Above 60% RH, the signal-to-noise ratio decreases substantially.

B. DNA on Mica. Figure 5 shows several double-stranded circular DNA molecules deposited on a mica surface. This image has been obtained at $V = 10$ V and $I = 1$ pA and an RH of 60%. The apparent dimensions of DNA are 1.5 and 15 nm for height

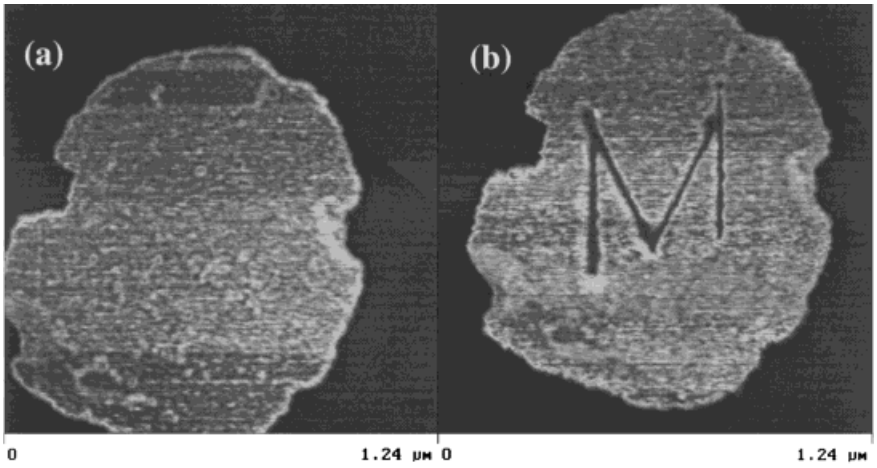

Figure 3. Current dependence experiments and modification of membranes. (a) STM image of a purple membrane. (b) Image after an *M* has been written on the membrane. The letter is generated by scanning at 20 pA. It implies the removal of the proteins in the modified region. In (a) and (b), $V = -7.7$ V; $I = 0.2$ pA; and RH = 37%. Scan size: 1.24×1.24 μm.

and width, respectively. In the context of scanning probe microscopic measurements of DNA, the small differences between observed and nominal DNA heights are remarkable. The apparent width is dominated by the tip–sample convolution.

Successful imaging is very sensitive to tip conditioning, applied voltage, set current, and RH. Stable images are obtained for RH in the 50–70% range, currents of $\leq$1 pA and high voltages (G. Zuccheri, R. García, and C. Bustamante, private communication).

The DNA is deposited onto a mica disk 1 cm in diameter with silver-painted electrodes at the edges, 2–3 mm away from the tip–sample interface. Mica is a good electrical insulator. Then, the charge transport from the tip to the silver electrode must involve ionic carriers. At 60% RH a continuous water layer of about 0.3 nm is adsorbed onto the mica surface.

Guckenberger et al. [21] reasoned that the water film on the surface of a hydrophilic insulator can be considered to function as a conductive coat, similar to the metal coat that is usually used for STM imaging of bulk insulators. They also studied the dependence of the current versus the tip–sample separation. Based on the exponential increase of the current when the tip is approached to the wetted mica surface, they proposed that the electrons go from the tip to the surface of the biomolecules through a tunneling process [30]. They also suggested that protons may be responsible for the charge transport from the surface of the molecules to the electrodes. Alternatively, Fan and Bard suggested that faradaic currents due to electrochemical reactions in the thin water film are responsible for the current [31]. The details of the imaging mechanism are still controversial, but the images reveal a novel high-resolution imaging mode based on ionic carriers.

IV. CONTRAST MECHANISM FOR IMAGING PM

For imaging DNA on mica and PM on graphite, high voltages and very low currents are required; however, there are also significative differences. The membranes are deposited on hydrophobic and conductive supports. Imaging of HOPG is independent of the RH.

In this section, we discuss a model that attempts to explain the origin of the contrast and its dependence with tip–substrate separation in PM experiments. There are two main components to the model: 1) field emission processes and 2) the electronic structure of the membrane.

To characterize the mechanism of image formation, I versus V curves have been measured. These curves show a linear dependence in the representation of $\log(I/V^2)$ versus $1/V$ [28]. This is characteristic of a field emission process described by Fowler–Nordheim equation,

$$I = AV^2 \exp\left(-6.85\ \phi^{3/2}\frac{S}{V}\right) \tag{1}$$

A is a factor that depends on the emitting area, V the applied voltage, S the tip–substrate distance, and ϕ the emitter work function; distances are in nanometers and energies in electron volts. Furthermore, I versus S gives effective barrier heights of 3.0 ± 0.5 eV. Those high values obtained in air also support a field emission process. As a comparison, the relationship between current, applied voltage, and tip–substrate separation in standard STM conditions (namely, when the voltage is smaller than the work function) is given by

$$I \propto V \exp(-10.25\ \phi S) \tag{2}$$

We conclude that when the tip is on the graphite, electrons are field-emitted. We consider unlikely to have an experimental situation where the current has two components, ions and electrons, one that applies when the tip is on the substrate and the other when the tip is on the membrane.

A realistic calculation of the electron transport through the biomolecule has to consider the complex electronic structure of the proteins within the membrane. This requires a computational power beyond our reach. However, insight about the contrast mechanism can be gained by using a simplified one-electron model for the electronic structure of proteins.

The protein is replaced by an energy potential with an effective work function ϕ_m, a pseudoband of empty states above the fermi

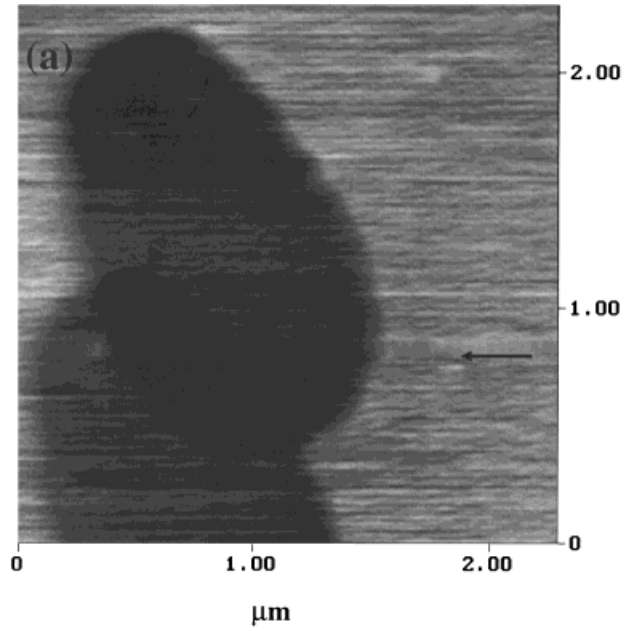

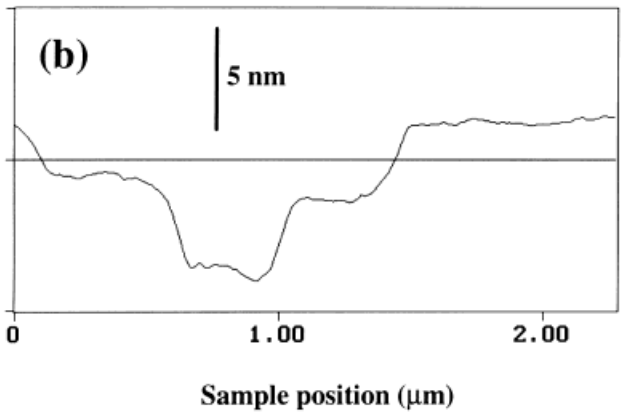

Figure 4. Negative contrast STM images of purple membranes. To keep the current constant the tip approaches toward the membrane. This approach is larger in the overlapping region (darker color). (b) Cross-section along the line indicated by the arrow in (a), $d_m \approx -3$ nm. $V = -6$ V; and $I = 0.09$ pA.

level of the substrate (ϕ_b), and a static dielectric constant (K_m) [Fig. 6(b)]. The observation of a wide absorption band centered around 2.2 eV above the occupied molecular orbitals in the protein [25] supports the pseudoband approximation. The effective barrier height could be related to the ionization potential of the protein. We use $\phi_m = 7.5$ eV and $\phi_b = 0.5$ eV, which would correspond to an ionization potential of 9.2 eV. The values of these parameters may affect the numerical results, but the behavior predicted by the model is not very sensitive to the values chosen. (Dielectric constants of proteins are not known with exactitude. Their estimated value is about 2–5. Here, a value of 4 is taken.)

The contrast of the images is quantified by measuring the apparent height d_m of the membranes. This is defined by

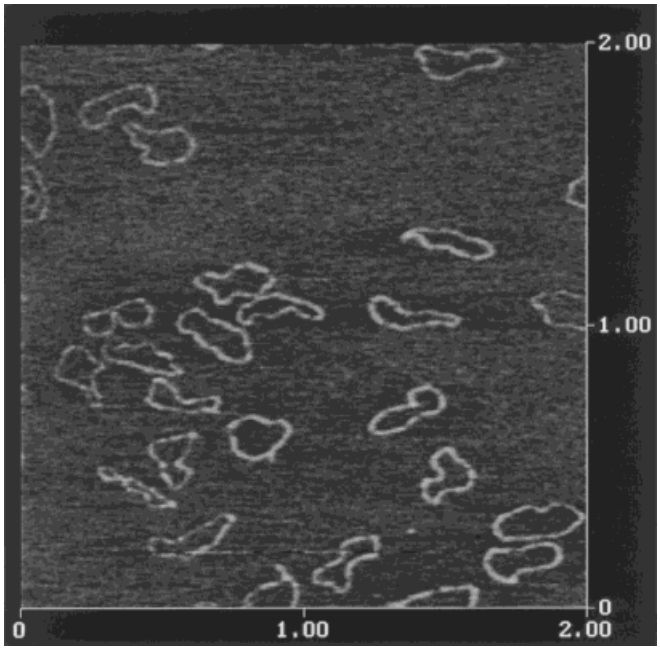

Figure 5. STM image of plasmid DNA adsorbed to mica. Scan size 2×2 μm. $V = 10$ V; $I = 1$ pA; and RH = 60%.

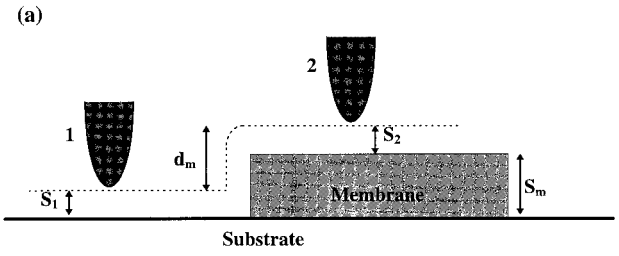

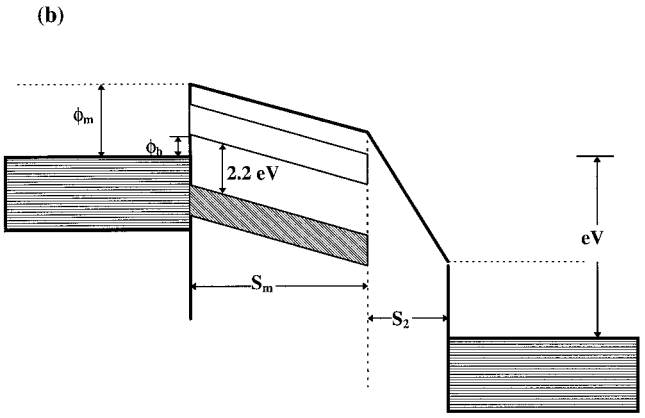

Figure 6. (a) Scheme of the experimental situation. The dashed line represents a hypothetical displacement of the tip when going from 1 (bare substrate) to 2 (over the membrane). (b) One-dimensional energy potential for the substrate–membrane–air gap–tip interface when there is an external voltage.

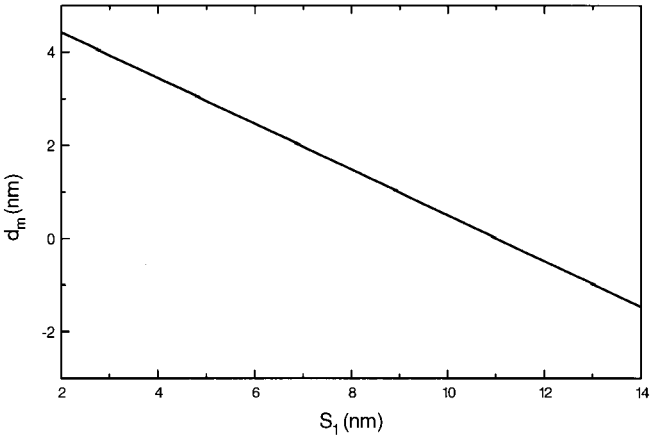

Figure 7. Apparent height versus tip–substrate separation. Positive values mean that the tip retracts when encountering the membrane. Negative values mean the tip moves toward the membrane. The calculation have been performed for $\phi_s = 5$ eV; $\phi_m = 7.5$ eV; $V = -8$ V; $K_m = 4$; and $S_m = 5$ nm.

$$d_m = S_m + S_2 - S_1 \tag{3}$$

where S_m is the nominal thickness of the membrane as measured by other techniques ($\sim$5 nm), and S_1 and S_2 are the tip–substrate and tip–membrane separations, respectively [Fig. 6(a)]. To calculate the dependence of the contrast with S_1, we suppose that the current does not change when the tip moves from the substrate to the membrane (these experiments are performed in the constant current mode). We also assume that when the tip is over the membrane the current is determined by the product of the transmission coefficients of the substrate–membrane and membrane–air interfaces. Each of these transmission coefficients is assumed to follow a Fowler–Nordheim-like law. In addition, the electrons propagate in the pseudoband as free particles, or follow paths similar to those in Ref. 32. From the above considerations and the continuity of the electrical field at the membrane surface, we deduce the following relationship between d_m and S_1 [20]:

$$d_m = \left[\frac{3\text{eV}}{2K_m}\frac{\phi_m^{1/2}}{(\phi_m^{3/2} + \phi_b^{3/2})} + 1 - K_m\right] S_m + \left[\frac{\phi_s^{3/2}}{(\phi_m^{3/2} + K_m\phi_b^{3/2})} - 1\right] S_1 \tag{4}$$

where ϕ_s is the work function of the substrate.

Figure 7 shows that the contrast (apparent height) has a linear dependence on the tip–substrate separation. A transition between negative and positive contrast is also present. The model reproduces the experimental observation that associates negative contrast with large tip–substrate separations. This behavior has its origin in the competition between the position of the empty states, the thickness of the membrane, and its dielectric constant for controlling the emission. $\phi_b < \phi_s$ tends to decrease the barrier when the tip is over the membrane with respect to the bare substrate. However, this effect may be compensated by $K_m > 1$, which decreases the voltage drop in the membrane, i.e., increases the barrier. What eventually tips the balance to positive or negative contrast is the electric field at the tip–membrane interface. The higher the field, the higher the contrast.

V. SUMMARY

In this article we have illustrated the use of the STM for imaging and selective nanometer-scale manipulation of biological membranes. The dominant parameters that control the imaging are the applied voltage, current density, and tip radius. We have imaged PM patches with vertical and lateral resolutions of 0.3 and 15 nm, respectively. The membranes can be properly imaged for set currents below 2 pA and applied voltages above 5.5 V, with negative polarities preferred. When both requirements are not met, to keep the current constant implies tip–membrane mechanical contact. This is often accompanied by disruption of the membrane and removal of the proteins by the tip. This effect can be exploited to generate nanometer-scale manipulations of biological membranes.

To explain the observed contrast, a model based on field emission and on the existence of empty states in the proteins is proposed.

Scanning tunneling microscopic reproducible imaging of biomolecules can be achieved by a variety of mechanisms involving electrons, protons, or ions. In terms of providing structural biological information, the STM seems less practical than force microscopy (see articles in this issue). The study of conductivity processes and the potential for manipulation of biomolecules at nanometer scale are perhaps the most attractive aspects of STM applications in biology.

ACKNOWLEDGMENTS

The authors thank G. Zuccheri for providing DNA images.

REFERENCES

1. H.-J. Güntherodt and R. Weisendanger, Eds., *Scanning Tunneling Microscopy,* Vols. 1 and 2, Springer-Verlag, Berlin, 1991; and references therein.
2. P. Avouris, Ed., *Atomic and Nanometre-Scale Modification of Materials: Fundamentals and Applications,* NATO ASI Series E, Vol. 239 (Kluwer Academic Press, Dordrecht, The Netherlands), 1993.
3. O. Marti and M. Amrein, Eds., *STM and SFM in Biology* (Academic Press, San Diego), 1993; and references therein.
4. N. J. Tao, J. A. DeRose, and S. M. Lindsay. ''Self-assembly of molecular superstructures studied by in situ scanning tunneling microscopy: DNA bases on AU(111),'' *J. Phys. Chem.* **97,** 910 (1993).
5. T. P. Beebe, T. E. Wilson, F. D. Ogletree, J. E. Katz, R. Balhorn, M. B. Salmeron, and W. J. Siekhaus. ''Direct observation of native DNA structures with the scanning tunneling microscope,'' *Science* **243,** 370–372 (1989).
6. M. Amrein, R. Durr, A. Stasiak, H. Gross, and G. Travaglini. ''Scanning tunneling microscopy of uncoated recA-DNA complexes,'' *Science* **243,** 1708 (1989).
7. M. E. Welland, M. J. Miles, N. Lambert, V. J. Morris, J. H. Coombs, and J. B. Pethica. ''Structure of the globular protein vicilin revealed by STM,'' *Int. J. Biol. Macromol.* **11,** 29 (1989).
8. M. J. Miles, H. J. Carr, T. J. McMaster, K. J. I'Anso, P. S. Belton, V. J. Morris, J. M. Field, P. R. Shewry, and A. S. Tatham. ''STM of a wheat seed storage protein reveals details of an unusual supersecondary structure,'' *Proc. Natl. Acad. Sci. USA* **88,** 68–71 (1991).
9. S. L. Tang and A. J. McGuie. ''Imaging individual chaperonin and immunoglobulin G molecules with scanning tunneling microscopy,'' *Langmuir* **12,** 1088–1093 (1996).
10. R. Guckenberger, W. Wiegrabe, A. Hillerbrand, T. Hartmann, Z. Wang, and W. Baumeister. ''Scanning tunneling microscopy of a

hydrated bacterial surface protein,'' *Ultramicroscopy* **31,** 327–332 (1991).
11. J. K. H. Hörber, F. M. Schuler, V. Witzemann, K. H. Schröter, H. Müller, and J. P. J. Ruppersberg. ''Imaging of cell membrane proteins with a scanning tunneling microscope,'' *Vac. Sci. Technol. B* **9,** 1214 (1991).
12. H. E.-M. Niemi, M. Ikonen, J. M. Levlin, and H. Lemmetyinen. ''Bacteriorhodopsin in Langmuir-Blodgget films imaged with a scanning tunneling microscope,'' *Langmuir* **9,** 2436–2447 (1993).
13. M. Maaloum, D. Chrétien, E. Karsenti, and J. K. H. Hörber. ''Approaching microtubule structure with the scanning tunneling microscope (STM),'' *J. Cell Sci.* **107,** 3127–3131 (1994).
14. D. P. E. Smith, J. K. H. Hörber, G. Binnig, and H. Nejoh. ''Structure, registry and imaging mechanism of alkylcyanobiphenyl molecules by tunneling microscopy,'' *Nature* **344,** 641–644 (1990).
15. W. Mizutami, M. Shigeno, M. Ono, and K. Kajimura. ''Voltage-dependent scanning tunneling microscopy images of liquid crystals on graphite,'' *Appl. Phys. Lett.* **56,** 1974 (1990).
16. J. K. Spong, H. A. Mizes, L. J. LaComb, Jr., M. N. Dovek, J. E. Frommer, and J. S. Foster. ''Contrast mechanism for resolving organic molecules with tunneling microscopy,'' *Nature* **338,** 137 (1989).
17. D. Dunlap, R. García, E. Schabtach, and C. Bustamante. ''Masking generates contiguous segments of metal-coated and bare DNA for STM imaging,'' *Proc. Natl. Acad. Sci. USA* **90,** 7652–7655 (1993).
18. D. D. Eley and D. I. Spivey. ''Semiconductivity of organic substances: Nuclei acid in dry state,'' *Trans. Faraday Soc.* **58,** 411 (1962).
19. B. Mann and H. J. Kuhn. ''Tunneling through fatty acid salt monolayers,'' *J. Appl. Phys.* **42,** 4398 (1971).
20. R. García, J. Tamayo, J. M. Soler, and C. Bustamante. ''Physical parameters that control the imaging of purple membranes with the scanning tunneling microscope,'' *Langmuir* **11,** 2109–2114 (1995).
21. R. Guckenberger, M. Heim, G. Cevc, H. Knapp, W. Wiegräbe, and A. Hillebrand. ''STM of insulators and biological specimens, based on lateral conductivity of ultrathin water films,'' *Science* **266,** 1538–1540 (1994).
22. D. Oesterhelt and W. Stoeckenius. ''Isolation of the cell membrane of Halobium halobium and its fractionation into red and purple membrane,'' *Methods Enzymol.* **31,** 667–678 (1974).
23. R. Henderson and P. N. T. Unwin. ''Three-dimensional model of purple membrane obtained by electron microscopy,'' *Nature* **257,** 2832 (1975).
24. D. J. Muller, F. Schabert, G. Büldt, and A. Engel. ''Imaging purple membranes in aqueous solutions at sub-nanometer resolution by atomic force microscopy,'' *Biophys. J.* **68,** 1681–1686 (1995).
25. D. Haronian and A. A. Lewis. *Appl. Optics* **30,** 597–608 (1991).
26. D. Dunlap, S. Smith, C. Bustamante, J. Tamayo, and R. García. ''A very low current scanning tunneling microscope,'' *Rev. Sci. Instrum.* **66,** 4876–4879 (1995).
27. R. M. Stiger, J. A. Virtanen, S. Lee, S. A. Virtanen, and R. M. Penner. ''Scanning tunneling microscopic observations of commensurate crystalline structures for horizontally deposited cadmium stearate bilayers on graphite,'' *Anal. Chem. Acta* **307,** 377–391 (1995).
28. R. García. ''Nanometer-scale modification of biological membranes by field emission scanning tunneling microscopy,'' *Appl. Phys. Lett.* **64,** 1162 (1994).
29. J. Tamayo, J. J. Sáenz, and R. García. ''Scanning tunneling microscopy modification of purple membranes,'' *J. Vac. Sci. Technol. A* **13,** 1737–1741 (1995).
30. M. Heim, R. Eschrich, A. Hillebrand, H. Knapp, G. Cevc, and R. Guckenberger. ''STM based on conductivity of surface adsorbed water. Charge transfer between tip and sample via electrochemistry in a water meniscus or via tunneling?,'' *J. Vac. Sci. Technol. B* **14,** 1498–1502 (1996).
31. F.-R. F. Fan and A. J. Bard. ''STM on wet insulators: Electrochemistry or tunneling?,'' *Science* **270,** 1849–1851 (1995).
32. R. García and N. García. ''Electron conductance in organic chains: why are STM experiments possible on bare biological samples?,'' *Chem. Phys. Lett.* **173,** 44–49 (1990).